Use of an Acousto-Optic Deflector Light Engine to Improve Resolution and Speed of the Stereolithography Process

Kaya J. Bayazitoglu[1], Tim Phillips[1], Joseph J. Beaman[1], Arthur Paolella[2], Carrigan Braun[2], James Ottaway[2], Chris Corey[2], Joe Dodd[2], Nick Alban[2]

[1]Center for Additive Manufacturing and Design Innovation and Department of Mechanical Engineering, University of Texas at Austin, Austin, TX, 78712

[2]Photonics and Quantum Sciences, L3Harris Technologies, Melbourne, FL, 32919

Abstract

In stereolithography (SLA) additive manufacturing (AM), a laser system creates part geometries using galvanometric mirrors and field lenses to locally polymerize raw materials. Small features require smaller laser spot sizes to achieve sufficient resolution and accuracy, while larger parts require longer scan times. The use of an acousto-optic deflector (AOD) to significantly reduce the time delay resolving the re-aiming of the laser to each disparate polymerization coordinate well below that of a galvo-system may allow for an increase in both speed and resolution of the SLA process. The use of an AOD to raster perpendicular to the regular galvo scan line enables the use of dynamic beam-shaping with smaller spot sizes while avoiding cure-through problems associated with the gaussian beam shape.

Introduction

In the stereolithography process, a laser and galvanometer (galvo) system is used to pattern ultraviolet (UV) light into a vat of polymer to selectively polymerize cross-sections (slices) of a part. The process of selectively energizing each slice is repeated many times to form a full 3D part.

Unfortunately, the speed of this process is fundamentally limited unless tradeoffs are made to part resolution. The spot size may range from 10 μm to 100 μm, and the galvo speed may go up to 10,000 mm/s. If higher speeds are desired, the laser irradiance (power per unit area) or spot size may be increased, enabling a greater rate of polymerization. However, these would both sacrifice part resolution, normal or in-plane to the slices respectively. The use of a galvo is advantageous because it is capable of large angular deflections, on the order of 10's of degrees, but as it is a moving system, it is subject to mechanical limitations.

Other attempts have been made to improve the speed limitations of the process. Jiang used a two-laser system, one with a 405 nm wavelength, and one with a 532 nm wavelength, to split the process between the outer contours and the internal crosshatch of the part. The 405 nm laser with its stronger penetration was used for contours and fine details, while the more powerful 532 nm laser was used for the internal crosshatch [1].

An acousto-optical deflector (AOD), shown in Figure 1, is an optical component that uses acoustic energy to manipulate its effective refractive index. A radio frequency (RF) signal is applied via an electrode to a transducer to propagate an acoustic wave through the AOD crystal. The photo-elastic effect generates periodic refractive index changes in the crystal, diffracting the first order beam to a determinable separation angle. Changes in the amplitude and frequency of

the RF signal affect the irradiance and direction of the first order output, respectively. Critically, the separation angle θ_S is primarily governed by the RF signal's frequency.

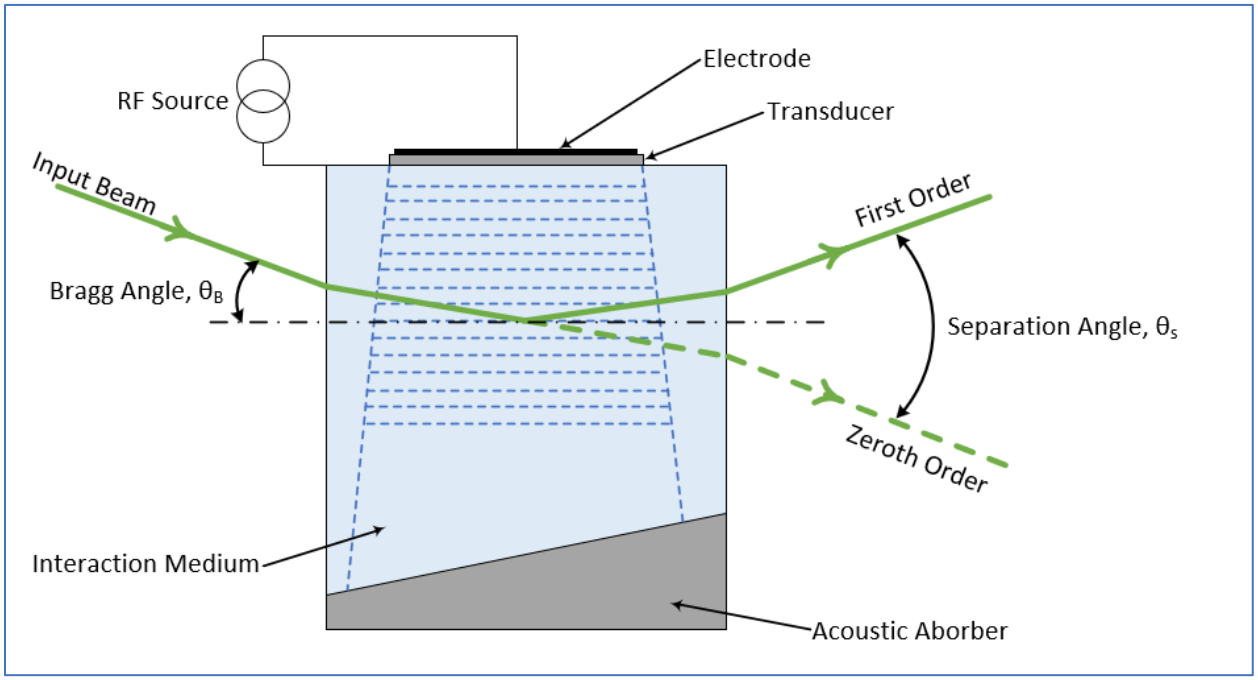

Figure 1: Acousto-Optical Deflector, the separation angle is primarily governed by the frequency of the RF signal

Because the AOD is a solid-state device, it provides a fast response rate, albeit within an angular range on the order of several milliradians. The use of two high-speed, low field-of-view AODs in series with a low-speed, high field-of-view galvo will maximize the advantages and minimize the disadvantages of both devices [2]. Figure 2 shows a component diagram of the selective laser additive manufacturing acousto light engine (SLAM-ALE) [3].

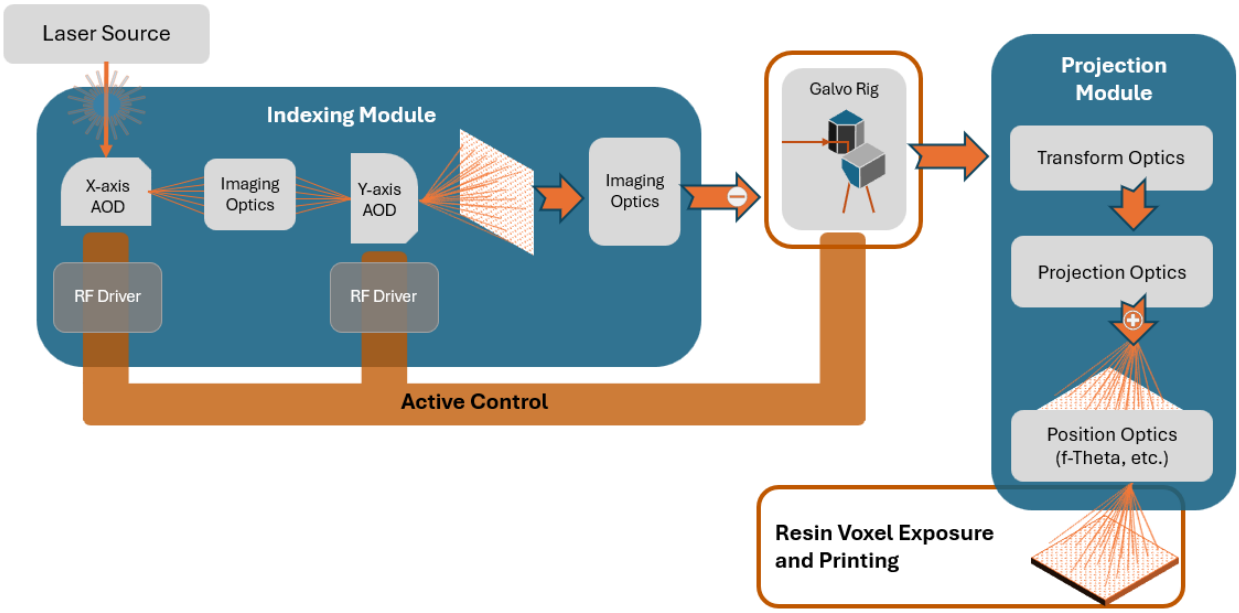

Figure 2: Selective two-dimensional AOD scan laser additive manufacturing acousto light engine component diagram

In the (2D) SLAM-ALE system, two AODs, one each for the x- and y-axes, scan the beam to create irradiance pattern for the galvo system to scan across the build plane surface, increasing manufacturing detail resolution and cure area without needing any modification to the galvo's sweep rate. Figure 3 depicts several one-dimensional (1D) galvo scans. One of a galvo operating alone, and two with a single AOD diffracting the laser perpendicular to the sweep direction of a single galvo mirror. The inclusion of the AOD increases the area covered by a single galvo sweep, increasing the possible speed of the process. The AOD scans at a rate sufficient to overlap adjacent lines, and its irradiance (curing power) can be switched on or off (blanked) to preserve spatial resolution. While the ability of the AOD system to provide blanking is a potentially powerful tool, and can happen on very short timescales, it is not instantaneous and will be the subject of future research.

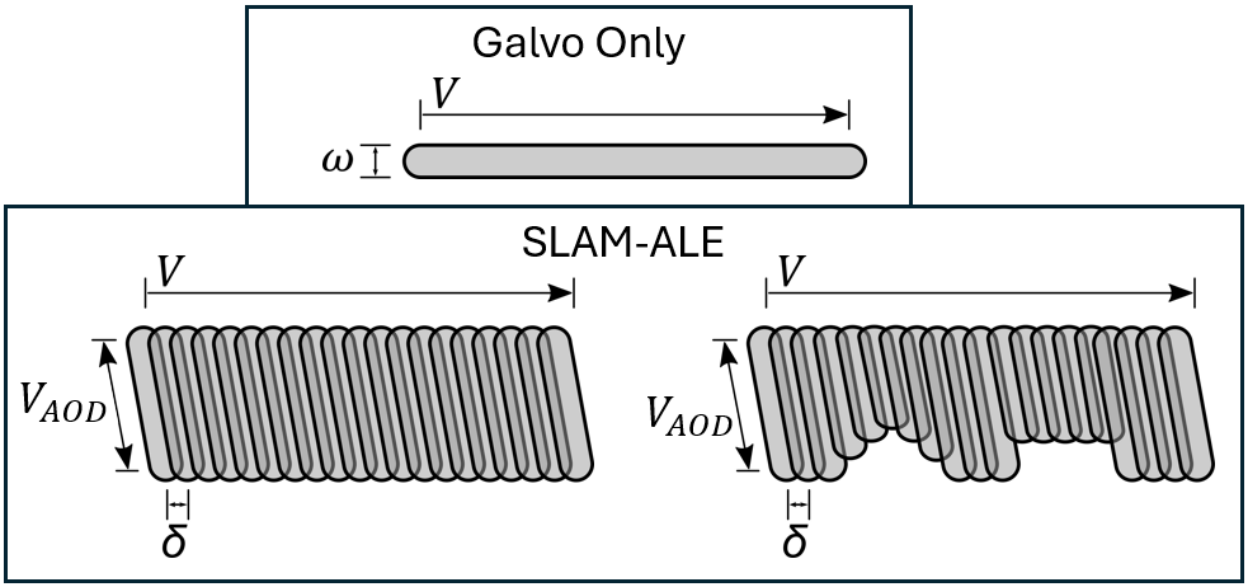

Figure 3: Top: single mirror 1D laser galvo scan polymerization; bottom left: 1D galvo + cross-directional AOD scan in modeled 1D SLAM-ALE system; bottom right: 1D galvo +cross-directional AOD scan with blanking

Table 1 compares the abilities of two similarly designed traditional SLA systems, one designed for part accuracy and the other designed for speed, with a hypothetical SLAM-ALE system. By covering the same area using fewer scans with the galvo, SLAM-ALE is capable of a 60% decrease in processing time compared to a high-speed system, while maintaining the same dimensional accuracy of the high-resolution system.

Table 1: Two galvo stereolithography systems compared to SLAM-ALE system

	Galvo – Dimensional Accuracy	**Galvo – High Speed**	**SLAM-ALE**
Laser spot size	10 µm	100 µm	10 µm + 100 µm
Scan speed	10 m/s	10 m/s	10 m/s + 500 m/s
Galvo scans in a 50-mm-wide path	12,500	1,250	500
Speed	✓	✓✓	✓✓✓
Resolution	✓✓✓	✓	✓✓✓

Laser Scan and Spacing Strategy

The beam energy of the laser is in the shape of a 3D Gaussian, simplified here to 2D for demonstration purposes. In the SLA process, adjacent scans must overlap one-another enough to produce a uniform energy profile. The overlap is defined in terms of the $1/e^2$ diameter, shown with an example of two adjacent beams in Figure 4.

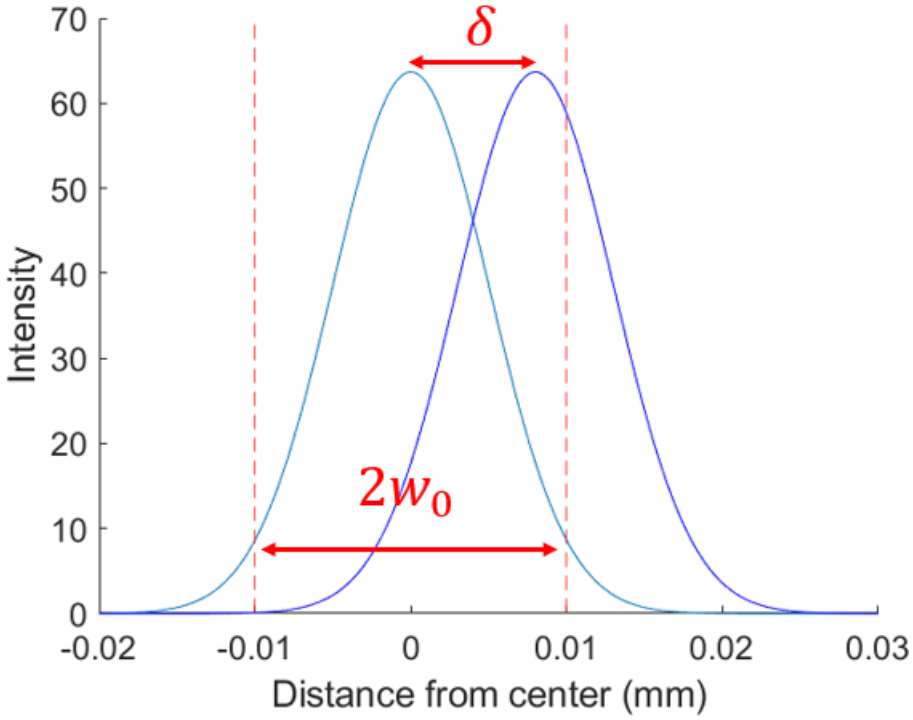

Figure 4: Two adjacent gaussian scans, with $1/e^2$ diameter and beam spacing

The beam spacing is described as the percentage of the beam width that overlaps with the adjacent beam.

$$\delta = (1 - overlap\%)\ 2w_0 \tag{1}$$

The resulting incident energy profile from many adjacent scan lines has been calculated, and two energy profiles are shown in Figure 5.

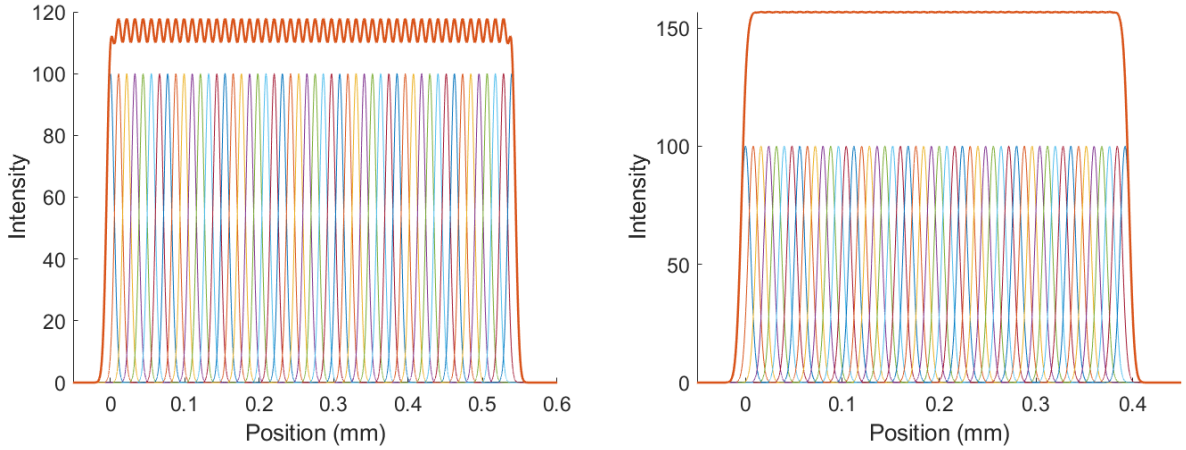

Figure 5: left: 45% overlap; right: 60% overlap

Adjacent scans should be spaced close enough to produce a smooth profile in the top-hat region in the middle of the beam. This can be quantified by finding the standard deviation in those regions. A plot of the standard deviation against the overlap percentage shown in Figure 6

shows that beyond 60% overlap, the returns of increasing the overlap diminish and 60% should be the target.

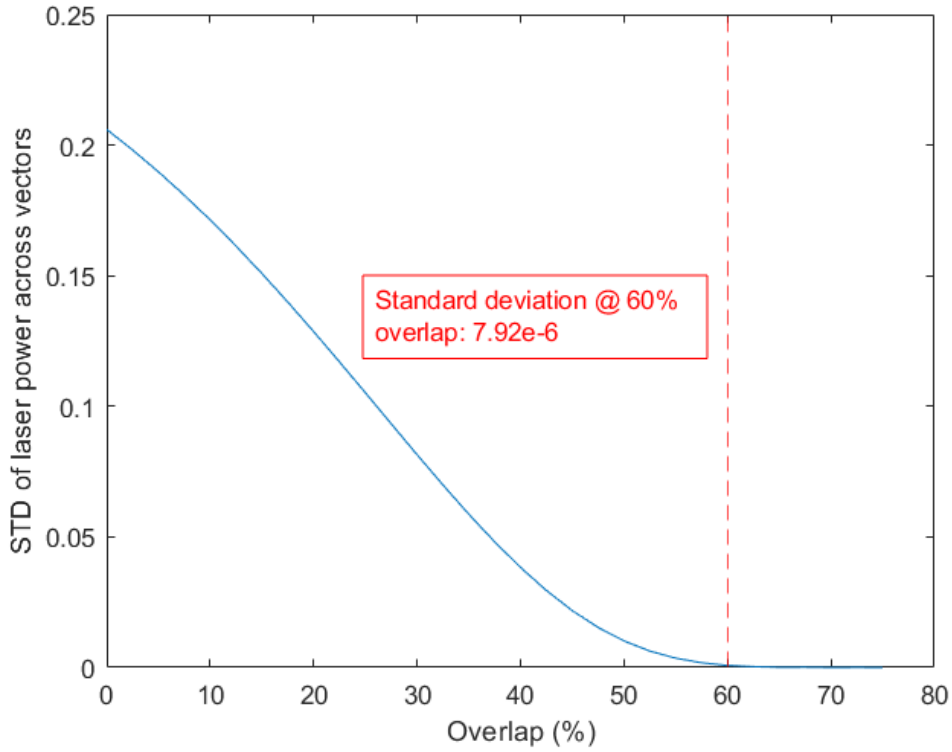

Figure 6: Standard deviation of top hat region vs overlap %

Simulation Methodology

Electromagnetic energy incident on the resin penetrates the surface, curing any volume wherein the deposited energy exceeds the resin's critical energy threshold. Adapted from Jacobs, the cure depth can be described using equation 2 [4].

$$C_d(x,y) = D_p * ln\left(\frac{E(x,y)}{E_c}\right) \tag{2}$$

C_d is the cure depth, D_p is the resin penetration depth, E_c is the resin's critical energy threshold, and E is energy incident on the surface of the resin. Equation 2 shows that the cure depth can be predicted with only the material properties of the resin and the energy incident at the surface.

The energy applied to the surface can be calculated in two ways. The first of these is using finite difference. At each time step, the beam position is determined and the energy at each surface level voxel is calculated using equation 3.

$$E(r) = E_{max} exp\left(-2\frac{r^2}{w_0^2}\right) \tag{3}$$

The calculated energies here are added to a running sum in the global simulation space.

$$E_{total} = \sum_{t=0}^{n} E_t \tag{4}$$

E_{total} in the above equation is the total energy applied to the surface of a voxel during the simulation and can now be used to find the cure depth at that location.

While the finite difference approach is powerful, it is computationally expensive, and a more efficient solution was required. Figure 7 depicts a beam, with the characteristic Gaussian irradiance profile, in a local coordinate space i, j, starting at i_0, j_0 and moving in the positive i direction.

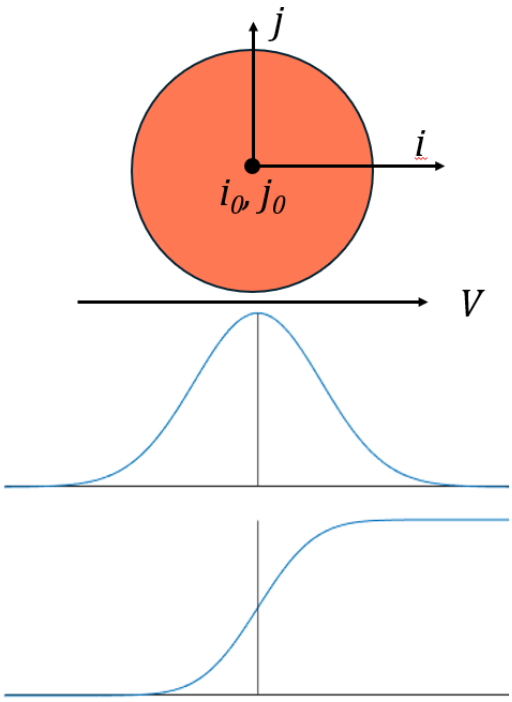

Figure 7: Top: beam starting at i_0, j_0 and moving in positive i direction; Middle: cross-section of the beam energy; Bottom: distribution of energy applied by moving beam

In statistics, a Gaussian distribution is an example of a normal probability distribution function (PDF). A cumulative distribution function (CDF) is often formed when it is desired to know the probability of a random number falling within a region of a PDF. Where x is a location on the PDF, the CDF is the integral of the PDF from -∞ to x, and in the case of the normal distribution, the error function is defined to describe the CDF of a normal distribution PDF. In the case of our moving beam, we want the energy deposited by a beam moving from a starting point to an end point. Knowing that the error function is the definite integral of a normal distribution, a solution in the form of equation 4 is developed.

$$E(i,j) = \left[\sqrt{\frac{1}{2\pi}}\frac{P_L}{w_0 V_i}\right]\left[exp\left(\frac{-2(j-j_0)^2}{w_0^2}\right)\right]\left[erf\left(\frac{2(i-i_0)}{w_0\sqrt{2}}\right) - erf\left(\frac{2(i-i_1)}{w_0\sqrt{2}}\right)\right] \quad (5)$$

The first bracket contains scan parameters. P_L is the laser power, w_0 is the beam width, and V_i is the beam speed in the positive-*i* direction. The second bracket describes the gaussian distribution of the beam energy in the *j*-direction. The third bracket contains two error functions. The first error function defines the start of the scan line at i_0, and the second defines the end at i_1. Together, they form an energy profile with error functions at each end, and a flat middle. The energy calculated here can now be added to the global simulation space similarly to the finite difference method using a simple coordinate transformation.

The finite difference method and the explicit solution can be combined in a simulation using the workflow shown in Figure 8.

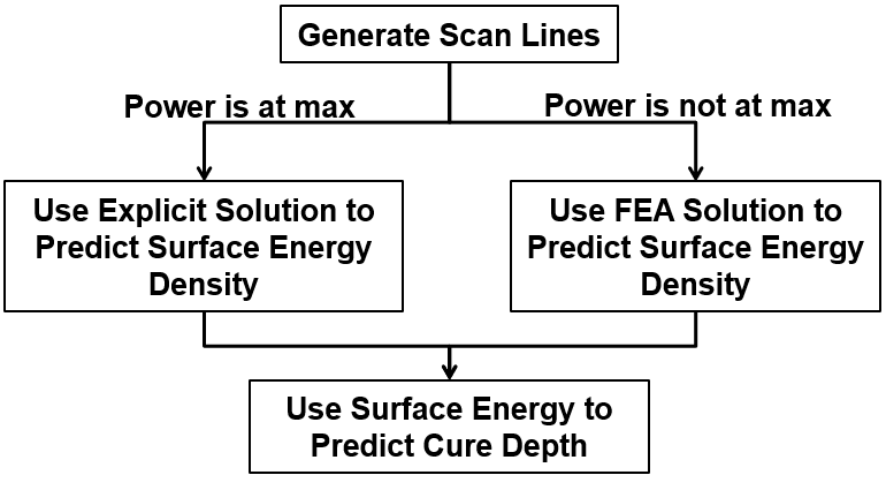

Figure 8: Basic simulation methodology

After generating a set of scan lines, they are sorted into regions of maximum power output and regions of changing power output. In regions of maximum power, the computationally efficient explicit solution is applied, and in other regions the finite difference method is used. Once the total energy applied to the surface across the simulation is found, the cure depth can be calculated.

Simulation Results

The simulation is developed to investigate the effects of processing parameters to predict the behavior of a future machine. A single galvo sweep with cross-axis AOD scans resembling **Error! Reference source not found.** is simulated using the simulation methodology.

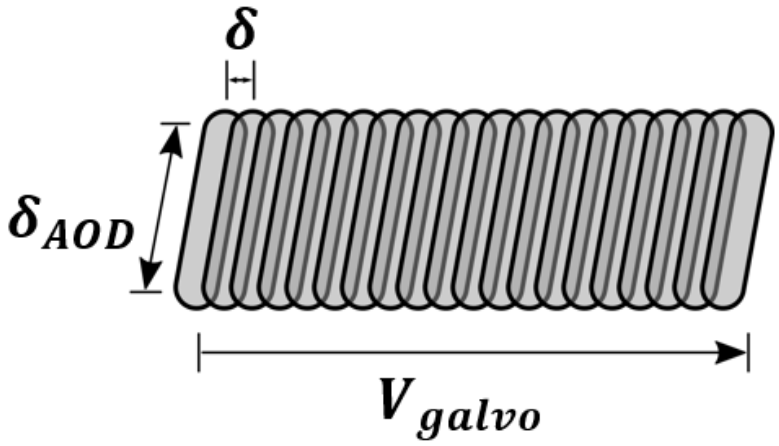

Figure 9: Simulated scan; δ_{AOD}: AOD scan range; δ: AOD scan spacing; V_{galvo}: galvo sweeping speed

The processing parameters under investigation are AOD scan rate, AOD scan range, laser power, spot size, and galvo sweeping speed. The spacing between adjacent scan lines must be controlled to maintain a uniform energy profile. The spacing between adjacent AOD scan lines, shown in Figure 9, can be controlled using the AOD scan rate and the galvo sweeping speed.

$$\delta = \frac{V_{galvo}}{f_{AOD}} \tag{6}$$

According to equations 1 and 6, the overlap percentage between scans is determined by the selection of beam width, AOD scan rate, and galvo sweeping speed.

An ideal set of parameters will produce a uniform cure depth and maximize build speed. Figure 10 illustrates a combination of parameters that gives a uniform cure depth across the area at the build plane. On the right of Figure 10 are the effects of modifying the individual parameters, and how they affect the uniformity and cure depth.

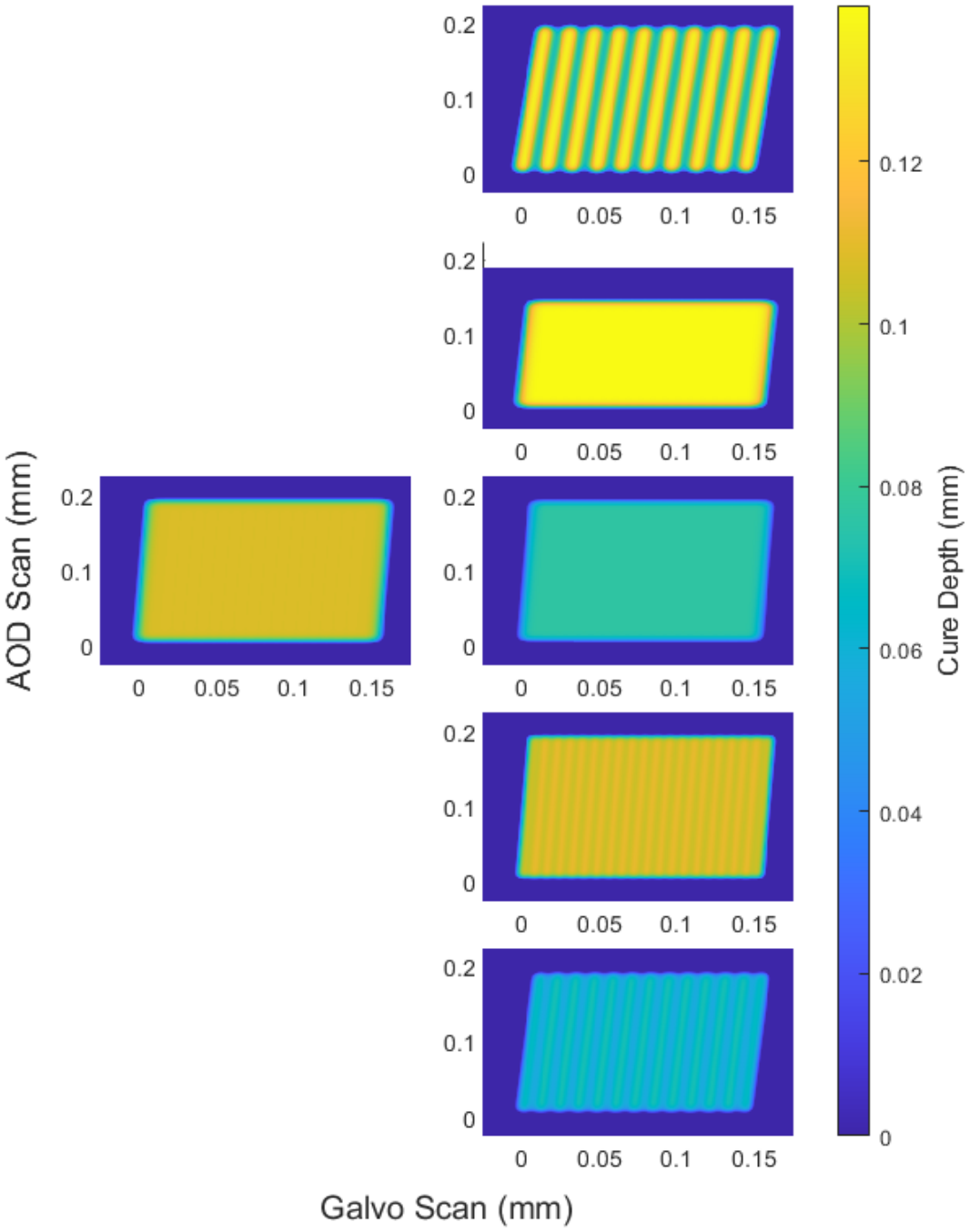

Figure 10: Left: effect of ideal parameters; Right in descending order: 125 kHz AOD scan rate, 1.5 mm AOD scan range, 75 mW laser power, 0.015 mm spot size, 3000 mm/s galvo sweeping speed

When the AOD scan rate is decreased, the AOD scan overlap decreases, and the cure depth is no longer uniform. Increasing the AOD scan rate increases the overlap between AOD scan lines, but increasing the overlap beyond 60% does not meaningfully improve cure depth uniformity. Decreasing the AOD scan range narrows the resultant galvo + AOD scan, focusing

the same energy into a smaller area and increasing the cure depth. Decreasing the laser power decreases the cure depth without any auxiliary effects.

Decreasing the spot size without adjusting the AOD scan rate or galvo sweeping speed lowers the AOD scan overlap, while increasing the spot size increases the AOD scan overlap. Decreasing the spot size would make a higher spatial resolution possible, but maintaining the cure depth uniformity would require a slower galvo sweeping speed or a higher AOD scan rate.

Increasing the galvo sweeping speed decreases AOD scan overlap and cure depth. Doing so would increase potential build speed, but an appropriate increase in AOD scan rate would be necessary to maintain AOD scan spacing, and an increase in laser power would be necessary to maintain cure depth.

Figure 11 shows the simulation results from the same good set of parameters shown in Figure 10. With a galvo sweeping speed of 2,000 mm/s, the AOD scan rate of 250 kHz and 0.02 mm spot size are sufficient to achieve a 60% overlap between AOD scans, and the laser power of 100 mW and the AOD scan range of 0.2 mm are selected to produce a cure depth of 0.108 mm.

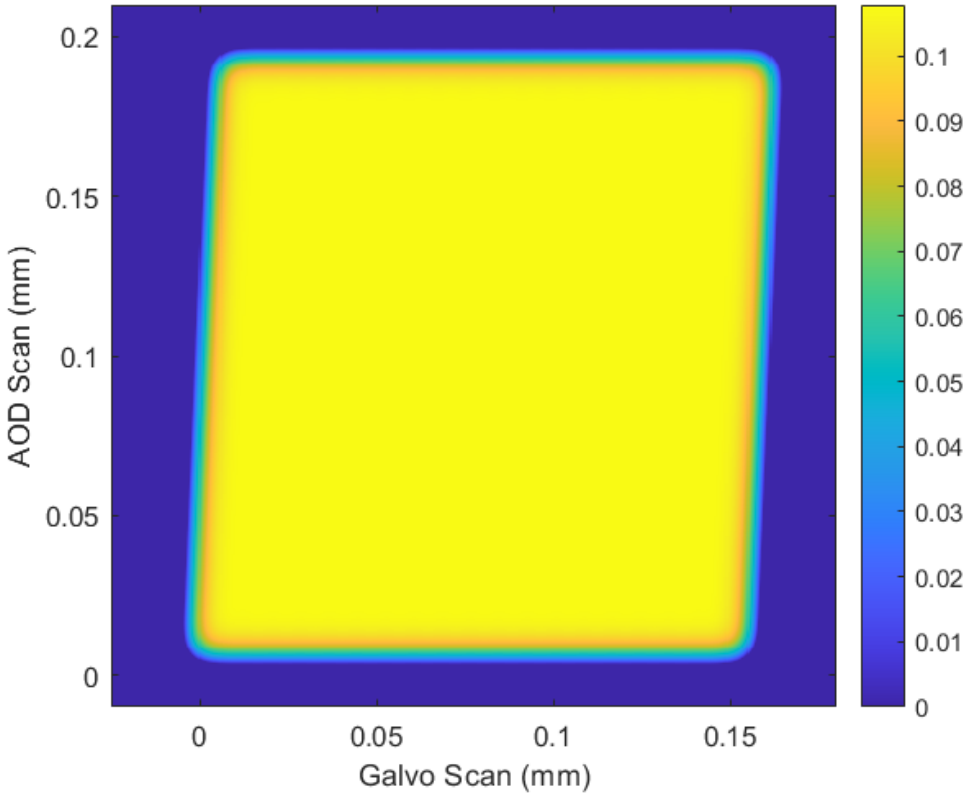

Figure 11: Results from a good set of parameters: 250 kHz AOD scan rate, 2 mm AOD scan range, 100 mW laser power, 0.020 mm spot size, 2000 mm/s galvo sweeping speed

Conclusion

The SLAM-ALE system is capable of significantly improving the speed of the stereolithography process, potentially by as much as 60% compared to a high-speed system, while maintaining the same resolution as a significantly slower system optimized for resolution. We developed a basic simulation to explore the processing parameters of a SLAM-ALE system and developed an ideal set of parameters to start with. In the future, we will further explore AOD blanking, which allows us to improve our processing speed without sacrificing spatial resolution. Ultimately, we will build an experimental system where we can validate the results of our simulation and experiment with processing parameters to optimize our process.

References

[1] C.-P. Jiang, "Accelerating fabrication speed in two-laser beam stereolithography system using adaptive crosshatch technique," *The International Journal of Advanced Manufacturing Technology,* vol. 50, pp. 1003-1011, 2010.

[2] P. B. G.R.B.E. Römer, "Electro-optic and Acousto-optic Laser Beam Scanners," *Physics Procedia,* vol. 56, pp. 29-39, 2014.

[3] C. A. Corey, R. K. Morse, P. A. Wasilousky, A. C. Paolella, C. L. Braun and C. D. Logan, "Additive manufacturing device with acousto-optic deflector and related methods". United States Patent US20220143905A1, 27 8 2024.

[4] P. F. Jacobs, "Fundamentals of Stereolithography," in *Solid Freeform Fabrication Symposium*, Austin, 1992.